Computational Particle Mechanics (2023) 10:519–531
https://doi.org/10.1007/s40571-022-00482-w

Numerical simulation of the flow characteristics around and through multiple porous particles

Mingyue Zhang[1] · Hui Jin[1] · Shaohua Shen[1]

Received: 27 February 2022 / Revised: 24 April 2022 / Accepted: 10 May 2022 / Published online: 1 September 2022

Abstract
Particle–fluid and particle–particle interactions can be widely seen in lots of natural and industrial processes. In order to understand these interactions, two-dimensional fluid flowing around and through nine porous particles was studied in this paper based on the lattice Boltzmann method due to its simplicity. Uniform spatial distribution and random spatial distribution were considered and the effects of Reynold number (Re), Darcy number (Da), and the distance between the particles (dx and dy) on the flow characteristics were analyzed in detail. The investigated ranges of the parameters were $10 \leq Re \leq 40$, $10^{-6} \leq Da \leq 10^{-2}$, $D \leq dx \leq 4D$ and $D \leq dy \leq 4D$ (D is the diameter of the particles). For uniform spatial distribution, it is observed that when$dx(dy)$ increases, the interactions between the particles become weak and the fluid can flow into the spacing between the particles. Besides, the average drag coefficient (C_{Dave}) increases with $dx(dy)$ increasing at $Re = 20$ and the increase rate gradually slows down. Furthermore, the distance change in the direction vertical to inflow direction has more obvious impact on the average drag coefficient. For example, for $Re = 20$ and $Da = 10^{-4}$, when dx equals D and dy increases from $2D$ to $3D$, C_{Dave} increases by 5.79%; when dy equals D and dx increases from $2D$ to $3D$, C_{Dave} increases by 2.61%.

Keywords Multiple porous particles · Uniform and random spatial distribution · Flow pattern · Lattice Boltzmann method · Drag coefficient

1 Introduction

Particle–fluid and particle–particle interactions can be widely seen in natural and industrial process and one particle and two particles models were usually investigated in experiments [1, 2] or simulations [3–10]. Though two particle model can be regarded as the simplest model for multi-particles flow which can reflect the interactions between particles to some extent, it also has great limitations. In order to understand the interactions between the particles and particles/fluid deeply, two-dimensional fluid flow around multiple particles should be studied.

Some scholars have analyzed the mechanical behavior of the particle clusters and the variation of drag coefficient. For example, O'Brien and Syamlal [11] carried out the experiments to consider the influences of particle clusters. The gas and particle drag law is modified by the experiments results. Sandeep and Zuritz [12] also conducted experiments to study the drag of single and multiple sphere assemblies in non-Newtonian fluid. The results show that when the particle concentration increases, the drag exerted on each sphere in assembly increases. And one equation was established to calculate the drag correction factor for the drag on a sphere in the assembly. Beetstra et al. [13] used the lattice Boltzmann method (LBM) to investigate the drag and flow characteristics of irregularly shaped (spherical, star-shaped, H-shaped, etc.) clusters. It is found that the drag coefficient of the particle clusters increases as the inter-particle distance increases for these shapes. And when a particle in the particle cluster is shielded by other particles in the flow direction, the particle's drag decreases. When the particles clusters become dispersed, the drag greatly increases. Shah [14] also used LBM model to investigate the influences of clusters on drag. They found that compared with random distribution, the particles in the cluster have a lower drag under the same simulation condition. With the total voidage increasing, the drag decreases and the decrease is evident for voidage higher than 0.7. Wei et al. [15] numerically quantified the interaction

✉ Shaohua Shen
shshen_xjtu@mail.xjtu.edu.cn

[1] State Key Laboratory of Multiphase Flow in Power Engineering, Xi'an Jiaotong University, Xi'an 710049, Shaanxi, People's Republic of China

between the gas and cluster and an empirical correlation was established. They discovered the clusters can significantly influence the flow field.

In above researches, the voidage/distance between the particles are considered, but the voids inside the spheres or particles are neglected. However, porous particles are general in industry such as gasification and there is little research about multiple porous particles. Compared with solid particles, porous particles allow fluid penetrating into them and the flow characteristics are very different. So it is necessary to investigate the flow characteristics around and through multiple porous particles. In addition, the lattice Boltzmann method was applied in these numerical simulations which indicates it is a good method to study the interactions between the particles and particles/fluid. And compared with traditional method, LBM is easy to handle complex geometries and it is widely used in porous media [16, 17]. Therefore, two-dimensional fluid flow around and through multiple porous particles was numerically investigated based on the LBM in this paper. Uniform spatial distribution and random spatial distribution were considered and the effects of *Re*, *Da* and the distance between the particles on streamlines and drag coefficient were analyzed in detail.

2 Numerical method

2.1 Governing equations

Darcy-Brinkman-Forchheimer model [18] can fully reflect the linear and nonlinear resistance term in the porous media and therefore was employed in this paper. And the following macroscopic governing equations [19] were used to describe fluid flow in the porous particles.

Continuity equation:

$$\nabla \cdot \langle u_f \rangle^f = 0 \tag{1}$$

Momentum equation:

$$\frac{\partial \langle u_f \rangle^f}{\partial t} + \langle u_f \rangle^f \cdot \nabla \langle u_f \rangle^f = -\frac{1}{\rho_f} \nabla \langle p_f \rangle^f + \upsilon \nabla^2 \langle u_f \rangle^f + F_n \tag{2}$$

where $\langle u_f \rangle^f$ is the intrinsic phase average velocity and can be defined as $\langle u_f \rangle^f = \frac{1}{V_f} \int_{V_f} u_f \mathrm{d}V$, and u_f is the velocity of the fluid, V is the representative volume and V_f is fluid volume within V. Similarly, $\langle p_f \rangle^f$ is intrinsic phase average pressure which can be defined as the same way of $\langle \boldsymbol{u}_f \rangle^f$. $\boldsymbol{F}_n$ is the total force, υ and ρ_f are the kinematic viscosity and density of the fluid, respectively. In order to simplify the writing and read easily, following we will use $\boldsymbol{u}$ to represent $\langle \boldsymbol{u}_f \rangle^f$.

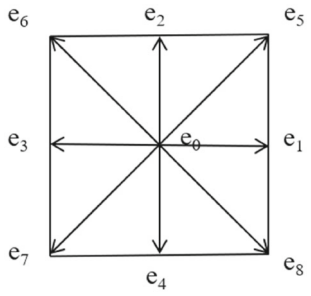

Fig. 1 D2Q9 model

2.2 Lattice Boltzmann method

2.2.1 Lattice Boltzmann (LB) governing equations

$$m_\alpha(\boldsymbol{x} + \boldsymbol{e}_\alpha \delta_t, t + \delta_t) - m_\alpha(\boldsymbol{x}, t) = -\frac{1}{\tau}\left[m_\alpha(\boldsymbol{x}, t) - m_\alpha^{\mathrm{eq}}(\boldsymbol{x}, t)\right] + \delta_t F_\alpha \tag{3}$$

where $m_\alpha(\boldsymbol{x}, t)$ is the density distribution function at position $\boldsymbol{x}$ and time t along α direction. D2Q9 lattice model [20] was employed as shown in Fig. 1 and $\boldsymbol{e}_\alpha$ can be written as follows:

$$\boldsymbol{e}_\alpha = \begin{cases} (0, 0) & \alpha = 0 \\ c\left(\cos\left[(\alpha - 1)\frac{\pi}{2}\right], \sin\left[(\alpha - 1)\frac{\pi}{2}\right]\right) & \alpha = 1, 2, 3, 4 \\ \sqrt{2}c\left(\cos\left[(2\alpha - 1)\frac{\pi}{4}\right], \sin\left[(2\alpha - 1)\frac{\pi}{4}\right]\right) & \alpha = 5, 6, 7, 8 \end{cases} \tag{4}$$

here c is the lattice speed and is defined by $c = \delta_x/\delta_t$, δ_x and δ_t are lattice step and time step, respectively.

On the right side of Eq. (3), the equilibrium density distribution function $m_\alpha^{\mathrm{eq}}(\boldsymbol{x}, t)$ and forcing term F_α are defined by

$$m_\alpha^{\mathrm{eq}}(\boldsymbol{x}, t) = \rho_f w_\alpha \left[1 + \frac{\boldsymbol{e}_\alpha \cdot \boldsymbol{u}}{c_s^2} + \frac{(\boldsymbol{e}_\alpha \cdot \boldsymbol{u})^2}{2c_s^4} - \frac{\boldsymbol{u}^2}{2c_s^2}\right] \tag{5}$$

$$F_\alpha = \rho_f w_\alpha \left(1 - \frac{1}{2\tau}\right)\left[\frac{\boldsymbol{e}_\alpha \cdot \boldsymbol{F}_n}{c_s^2} + \frac{\boldsymbol{e}_\alpha \cdot \boldsymbol{u}}{c_s^4}(\boldsymbol{e}_\alpha \cdot \boldsymbol{F}_n) - \frac{\boldsymbol{u} \cdot \boldsymbol{F}_n}{c_s^2}\right] \tag{6}$$

where w_α is the weighting factor and in D2Q9 model, $w_0 = 4/9$, $w_{1-4} = 1/9$, $w_{5-8} = 1/36$. $c_s = c/\sqrt{3}$ is sound speed.

The total force $\boldsymbol{F}_n$ in Eqs. (2) and (6) is expressed as

$$\boldsymbol{F}_n = -\frac{\varepsilon \nu}{K}\boldsymbol{u} - \frac{\varepsilon^2 F_\varepsilon}{\sqrt{K}}\boldsymbol{u}|\boldsymbol{u}| \tag{7}$$

where ε and K are porosity and permeability, respectively. Geometry function $\boldsymbol{F}_\varepsilon$ and kinematic viscosity ν can be calculated as follows:

$$\boldsymbol{F}_\varepsilon = \frac{1.75}{\sqrt{150\varepsilon^3}} \tag{8}$$

$$\nu = c_s^2(\tau - 0.5)\delta_t \tag{9}$$

here τ is relaxation time.

Furthermore, the density and velocity can be calculated from the density distribution function $m_\alpha(\boldsymbol{x}, t)$:

$$\rho_f = \sum_\alpha m_\alpha(\boldsymbol{x}, t) \tag{10}$$

$$\rho_f \boldsymbol{u} = \sum_\alpha \boldsymbol{e}_\alpha m_\alpha(\boldsymbol{x}, t) + \frac{1}{2}\delta_t \rho_f \boldsymbol{F}_n \tag{11}$$

Combined Eqs. (7) and (11), $\boldsymbol{u}$ can be calculated by

$$\boldsymbol{u} = \frac{\boldsymbol{v}}{q_0 + \sqrt{q_0^2 + q_1|\boldsymbol{v}|}} \tag{12}$$

where temporary velocity $\boldsymbol{v}$ is defined as

$$\rho_f \boldsymbol{v} = \sum_\alpha e_\alpha m_\alpha(\boldsymbol{x}, t) \tag{13}$$

The parameters q_0 and q_1 in Eq. (12) are defined by

$$q_0 = \frac{1}{2}\left(1 + \frac{\delta_t}{2}\frac{\varepsilon\nu}{K}\right),\ q_1 = \frac{\delta_t}{2}\frac{\varepsilon^2 F_\varepsilon}{\sqrt{K}} \tag{14}$$

2.2.2 Dimensionless parameters

(1) Reynolds number
The Reynolds number (Re) used in this study is defined by:

$$Re = \frac{u_\infty D}{\nu} \tag{15}$$

where u_∞ is the velocity of the fluid at the inlet and D is the diameter of the porous particles.

(2) Darcy number
The Darcy number (Da) can be evaluated from the Carman-Kozeny relation [21],

$$Da = \frac{K}{D^2} = \frac{1}{180}\frac{\varepsilon^3 d_p^2}{D^2(1-\varepsilon)^2} \tag{16}$$

here d_p is the diameter of a particle in the porous aggregate.

(3) Drag coefficient and lift coefficient
The momentum exchange method [22] is applied to obtain the total fluid force $\boldsymbol{F}_T$ acting on one porous particle:

$$\boldsymbol{F}_T = \sum_{all\boldsymbol{x}_b}\sum_{\alpha\neq 0} \boldsymbol{e}_\alpha \left[m_\alpha(\boldsymbol{x}_b, t) + m_{\overline{\alpha}}(\boldsymbol{x}_b + \boldsymbol{e}_{\overline{\alpha}}\delta t, t)\right] \times \left[1 - w\left(\boldsymbol{x}_b + \boldsymbol{e}_{\overline{\alpha}}\delta t\right)\right] \tag{17}$$

where x_b is the boundary node of the porous particle and $m_{\overline{\alpha}}$ is the density distribution function with $\boldsymbol{e}_{\overline{\alpha}} = -\boldsymbol{e}_\alpha$. There are two values of $w(i,j)$: zero at fluid nodes and one at porous particle nodes.
The drag coefficient (C_D) and lift coefficient (C_L) are obtained from the total fluid force.

$$C_D = \frac{F_x}{0.5\rho_f U_{\text{ref}}^2 L_{\text{ref}}} \tag{18}$$

$$C_L = \frac{F_y}{0.5\rho_f U_{\text{ref}}^2 L_{\text{ref}}} \tag{19}$$

here F_x is x-component and F_y is y-component of the force $\boldsymbol{F}_T$. U_{ref} and L_{ref} are the characteristic velocity and characteristics length, respectively. The characteristic velocity we used here is the inlet velocity of the fluid and the characteristic length is the diameter of the porous particle.

(4) Average drag coefficient and average lift coefficient
In addition, the average drag coefficient (C_{Dave}) and average lift coefficient (C_{Lave}) can also be calculated by:

$$C_{\text{Dave}} = \frac{1}{N}\sum_{i=1}^{N} C_{Di} \tag{20}$$

$$C_{\text{Lave}} = \frac{1}{N}\sum_{i=1}^{N} C_{Li} \tag{21}$$

where N is the quantity of all porous particles. C_{Di} and C_{Li} are the drag coefficient and lift coefficient of the i-th porous particle.

2.3 Computational domain

Steady flow around and through multiple porous particles was studied numerically. Uniform and random spatial distributions were considered in the paper and here we took uniform spatial distribution as an example to illustrate the computational domain as depicted in Fig. 2. The diameters of the particles were D. The quantity of the porous particles (N) was nine and the column (p) and row (q) of the particles

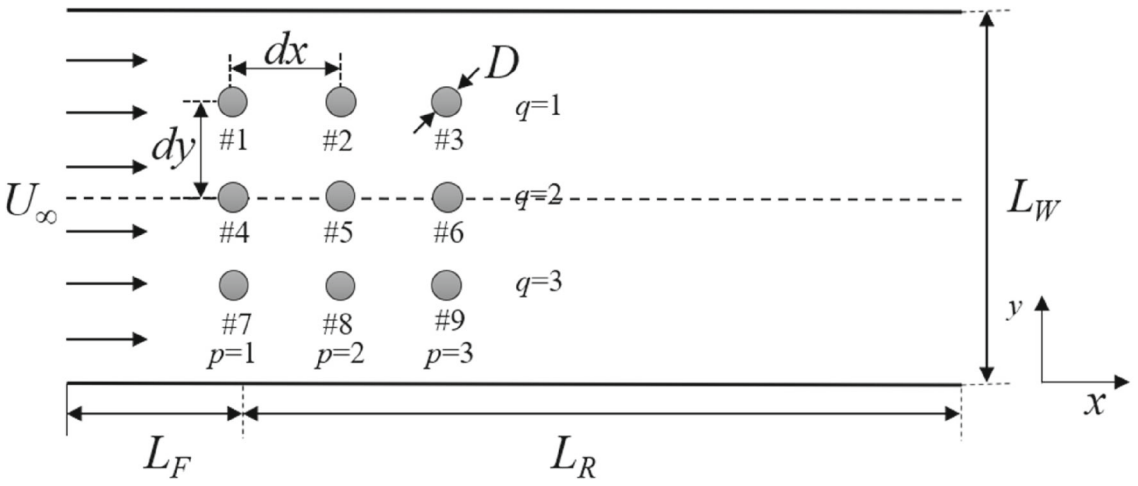

Fig. 2 Computational domain and particles' serial numbers

Table 1 Test of the mesh independence at $Re = 20$, $Da = 10^{-3}$ and $dx = dy = 2D$

Mesh	Grids numbers	C_{Dave}	Relative error (%)
1	1200 × 900	1.398	/
2	1600 × 1200	1.395	0.22
3	2000 × 1500	1.393	0.14

are both three. The distance between the first column and the inlet and outlet were L_F and L_R and the distance between the particles in x direction and y direction were dx and dy. The particles were symmetrically distributed in y direction. Fluid flowed into the computational domain with a uniform velocity U_∞ and was fully developed at the outlet boundary. Besides, non-slip boundary condition was imposed on the top and bottom wall. For the convenience of analysis, the particles' serial numbers were also shown in Fig. 2.

2.4 Validation

Because the grids numbers can greatly affect the accuracy of the simulation results, several meshes were chosen to test the independence of the mesh. Fluid flow around nine ($p = q = 3$) particles with the same diameter and permeability as shown in Fig. 2 was simulated and the distance between the particles was $2D$ ($dx = dy = 2D$). The test Reynolds number and Darcy number were 20 and 10^{-3}, respectively. The average drag coefficients and relative errors of the meshes are shown in Table 1. From the table, we can see the relative error between Mesh 1 and Mesh 2 was 0.22% and the relative error between Mesh 2 and Mesh 3 was 0.14%. Therefore, considering the computation resources and accuracy, Mesh 2 was chosen to carry out all simulations in this paper. Under this grid size, the particles' diameter D expressed by the number of grids is 40.

Because there is little research about multiple porous particles, the method was applied to simulate fluid flow around one particle to test the accuracy. Let $p = q = 1$ and there is only one particle in the computational domain. The porous particle was at the center of y-axis with distances of L_F and L_R to the inlet and outlet boundary. The comparison of drag coefficient at different values of Re and Da is depicted in Fig. 3. We can see that the simulated results were in good agreement with the results in the previously published literatures [2, 3, 6, 9, 10]. Therefore, it is concluded that the method can be used to simulate fluid flow around and through porous particles accurately.

3 Results and discussions

In the present study, fluid flow around and through nine porous particles was investigated numerically within the following parameter ranges: $10 \le Re \le 40$, $10^{-6} \le Da \le 10^{-2}$, $D \le dx \le 4D$, $D \le dy \le 4D$.

Several situations were considered and the effects of above parameters on the flow characteristics were analyzed in detail.

3.1 Particles with uniform spatial distribution

3.1.1 The streamlines analysis with $dx = dy$

Fluid flowing around nine ($p = q = 3$) identical (same diameter and permeability) porous particles was simulated to analyze the influences of Re, Da and the distances between the particles (dx and dy). Firstly, the particles were uniformly

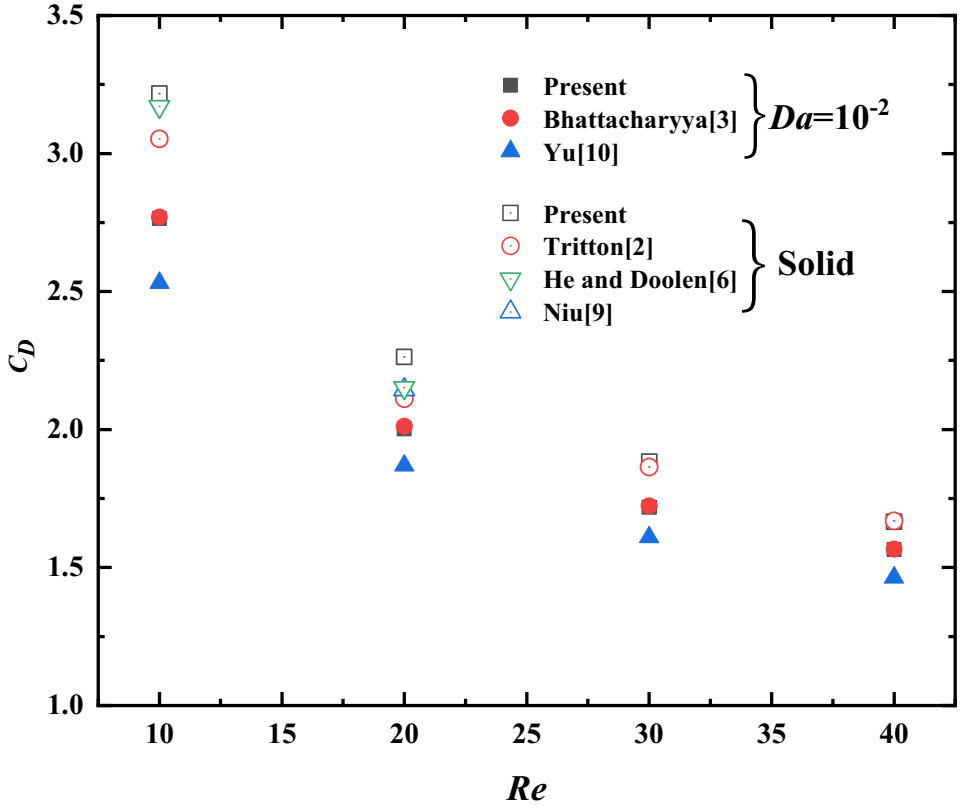

Fig. 3 The comparison of drag coefficient of one particle

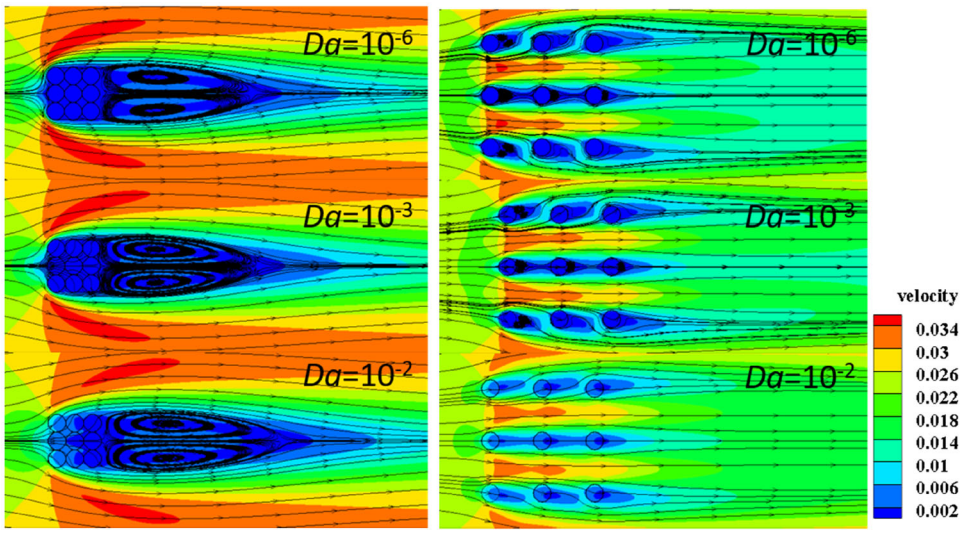

(a) dx=dy=D (b) dx=dy=3D

Fig. 4 The streamlines for the flow around and through nine identical porous particles at $Re = 20$ for **a** $dx = dy = D$ and **b** $dx = dy = 3D$

distributed and the distance between the particles in the x and y direction were the same ($dx = dy$).

Figure 4 shows the streamlines for the flow around and through nine identical porous particles at $Re = 20$ for $dx = dy = D$ and $dx = dy = 3D$. It is observed that when $Da = 10^{-6}$, there is little fluid penetrating through the particles and almost all fluid flow around the particles. In other words, the flow patterns of the porous particles at $Da = 10^{-6}$ are similar to those of impermeable solid particles and the porous particles can be regarded as solid particles. When Da increases, the resistance of the particles to the fluid decreases and the fluid can flow through the permeable particles. Besides, the larger the Darcy number, the smaller the degree of fluid deviation in the particles.

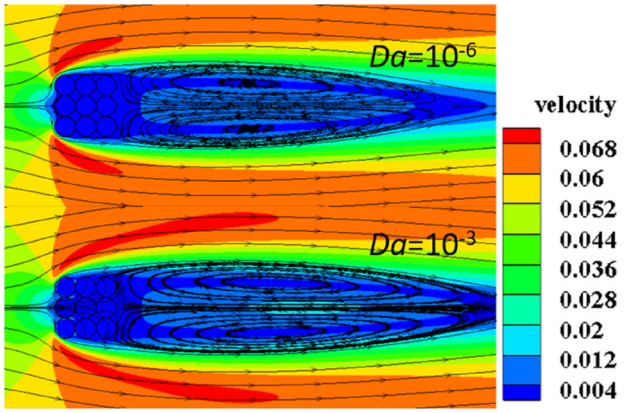

Fig. 5 The streamlines for the flow around and through nine identical porous particles at $Re = 40$ and $dx = dy = \mathrm{D}$

For $dx = dy = D$, the distance between the particles are small and the fluid is difficult to enter the gap between the particles. Besides, the particles form a cluster which has a great interference to the fluid and two recirculating symmetrical wakes are formed behind the cluster at different values of Da. When the distance increases, the particles are dispersed and can't be regarded as a cluster. As depicted in Fig. 4b, when dx and dy increases to $3D$, most fluid flows through the space between the particles with low resistance due to the larger inter-particle distance, especially when the Darcy number is low. This is because at high Darcy number, the resistance of porous particles to the fluid is small. And the distribution of the particles is dispersed which no longer exerts an overall influence on the fluid like the particle cluster. The flow characteristics of the fluid around each particle are different. At $Da = 10^{-6}$, two wakes are formed behind the particles at $p = 1$. For #4, because it is situated at the center of y-axis, two symmetrical wakes are formed. But for #1 and #7, two asymmetrical wakes are formed behind them. Furthermore, the particles at $p = 1$ have significant effects on the particles at $p = 2$ and $p = 3$. Similarly, #4 is situated at the symmetric axis in y direction and when fluid flow around it, the fluid keep symmetrical. As a result, two symmetrical wakes are also formed behind #5 and #6. Compared with #4, #1 and #7 cause a larger fluid deflection when fluid flow around them and therefore, no wake is formed behind #2, #3, #8 and #9. When Da increases, the fluid can penetrate into the particles and the interference to the fluid is reduced. At $Da = 10^{-2}$, the wakes behind all particles vanish totally.

In order to better understand the influences of Reynolds number, the streamlines at $Re = 40$ and $dx = dy = D$ are plotted as shown in Fig. 5. Compared with Fig. 4a, it is observed as Re increases, the symmetrical wakes behind the cluster increase obviously due to the increase in inertial force and the phenomenon can also been seen in the situation where fluid flow around one porous particle.

3.1.2 The average drag coefficient analysis with $dx = dy$

Figure 6 shows the average drag coefficient of the nine identical porous particles at $Re = 20$ and 40 for different values of $dx(dy)$. It is observed that the average drag coefficient increases with $dx(dy)$ increases at $Re = 20$. Because as the distance between the particles increases, the shading effect of the front particles on the rear particles reduces. Besides, we can also see that when $dx(dy)$ increases, the growth rate

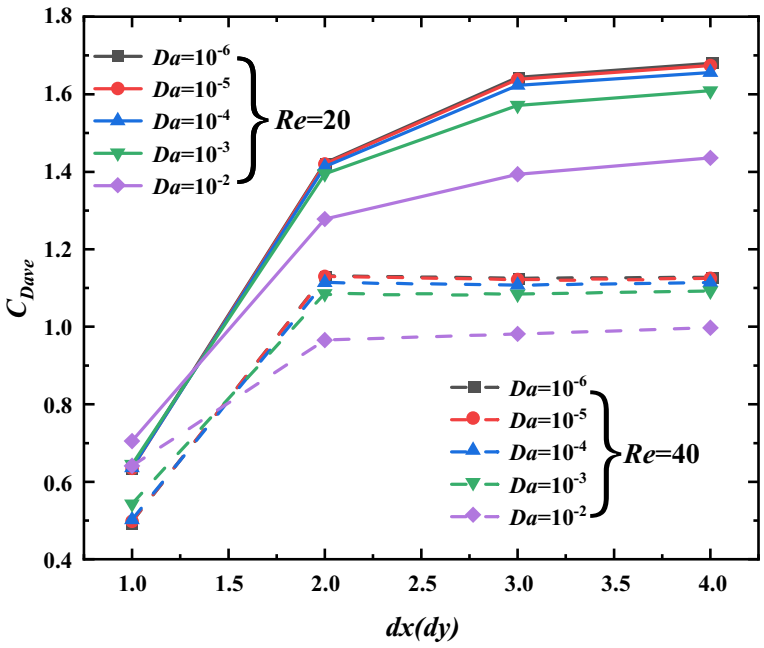

Fig. 6 The average drag coefficient for the flow around and through nine identical porous particles at $Re = 20$ and 40 for different values of $dx\ (dy)$

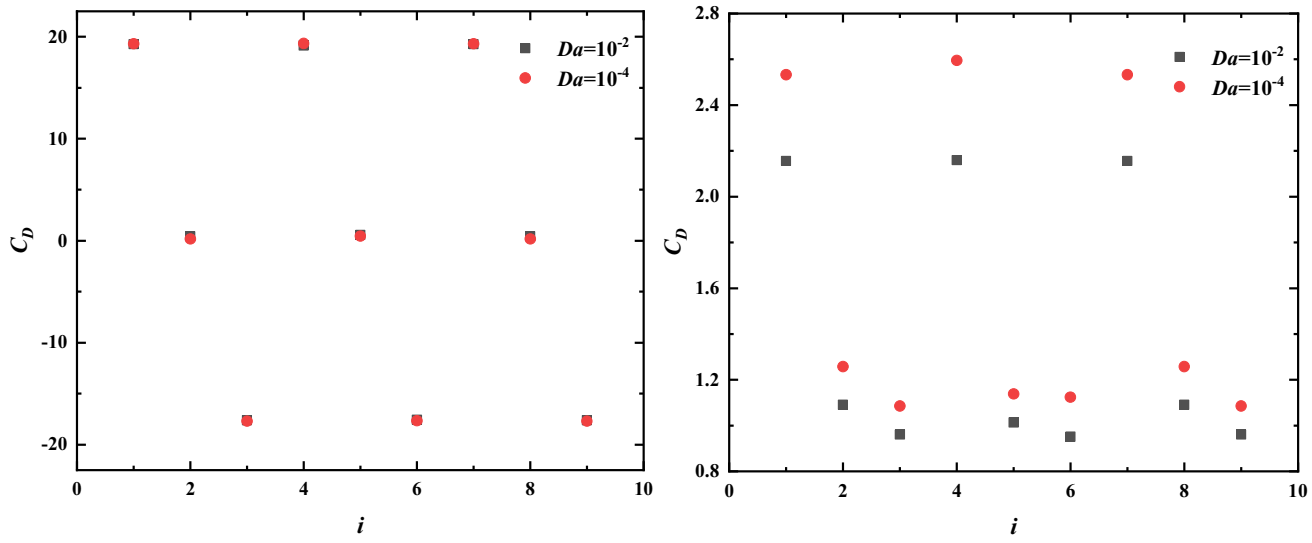

Fig. 7 The drag coefficient of the nine identical porous particles at $Re = 20$ for **a** $dx = dy = D$ and **b** $dx = dy = 3D$

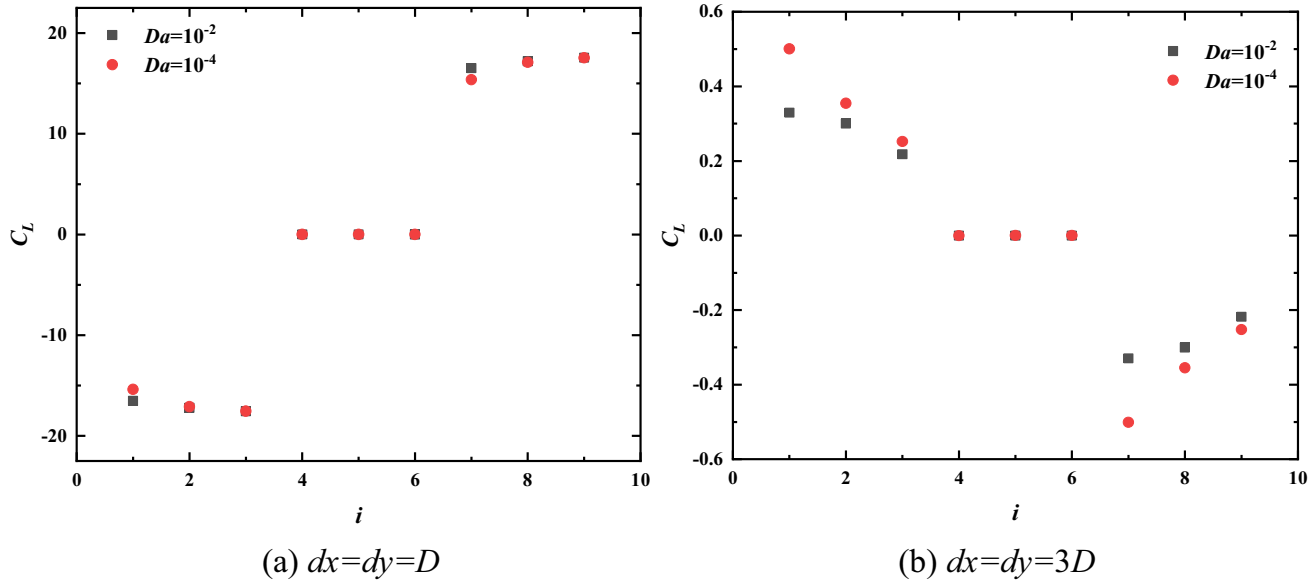

Fig. 8 The lift coefficient of the nine identical porous particles at $Re = 20$ for **a** $dx = dy = D$ and **b** $dx = dy = 3D$

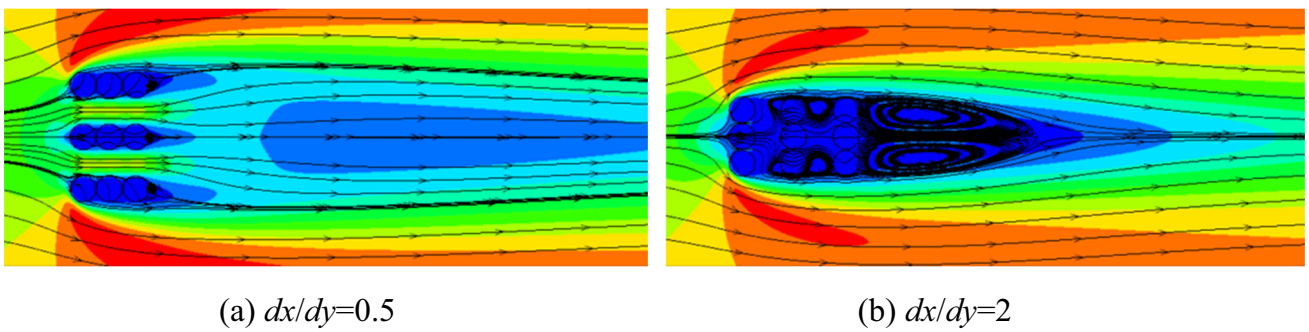

Fig. 9 The streamlines of nine identical porous particles at $Re = 20$ and $Da = 10^{-3}$ for **a** $dx(dy) = 0.5$ and **b** $dx(dy) = 2.0$

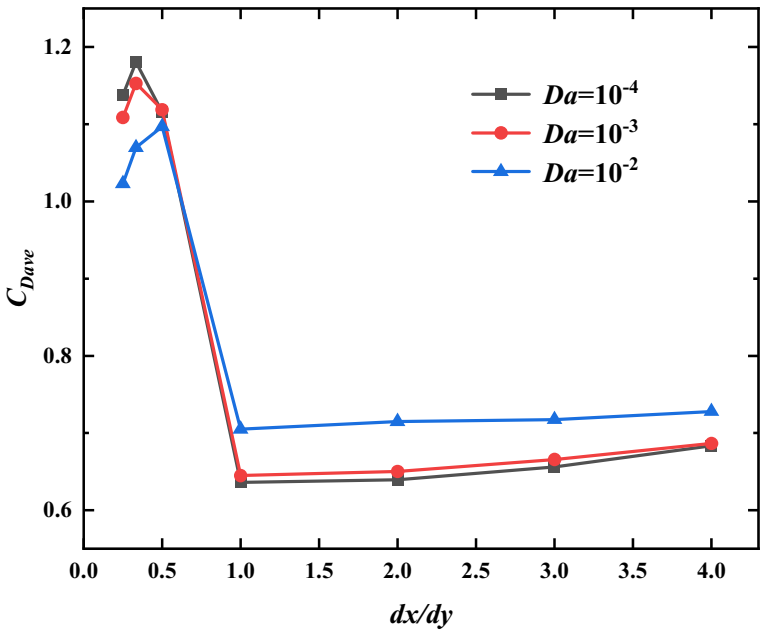

Fig. 10 The average drag coefficient of nine identical porous particles at $Re = 20$ for different values of Da and $dx(dy)$

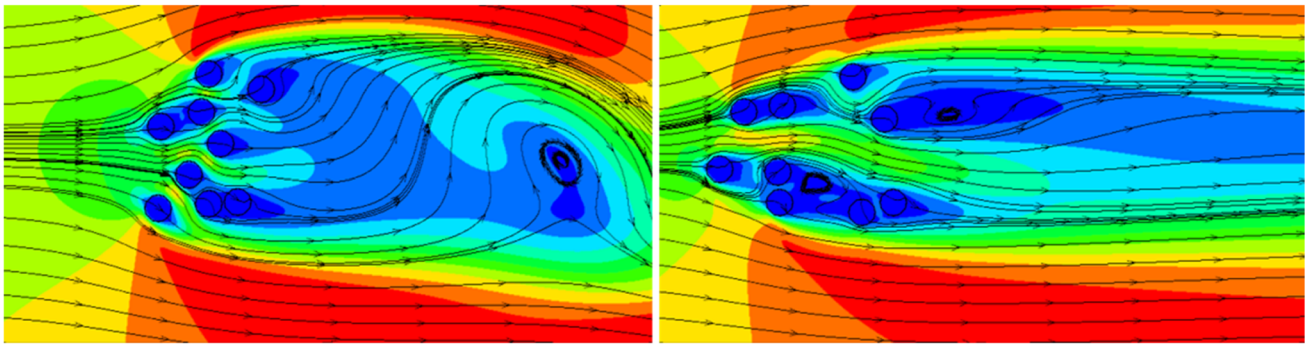

Fig. 11 The streamlines of nine identical porous particles with random distribution at $Re = 20$ and $Da = 10^{-3}$

of C_{Dave} slows down which indicates the influences of $dx(dy)$ gradually decrease. It is expected when the distance increases to a certain value, the average drag coefficient will reach a maximum value and then remains unchanged. At $Re = 40$, C_{Dave} increases for $D \le dx(dy) \le 2D$ and almost keeps constant for $2D \le dx(dy) \le 4D$. That indicates the effects of $dx(dy)$ decrease as the inertial force increases. Furthermore, under the same Da and $dx\ (dy)$, C_{Dave} is in a reduction with Re increasing.

When Darcy number increases, the resistance of the particles on the fluid reduces, and therefore, the average drag coefficient decreases for $2D \le dx(dy) \le 4D$. At $dx = dy = D$, like the analysis in Sect. 3.1, the particles form a cluster and the influences of multiple particles on the fluid are presented as the overall effect of the cluster on the fluid. Therefore, for $10^{-6} \le Da \le 10^{-3}$, the average drag coefficient of the particles almost remains unchanged with Da increasing and only at $Da = 10^{-2}$, C_{Dave} increases a little. However, compared with the increase resulted from Darcy number at other $dx(dy)$, this increase can be ignored.

At $Re = 20$, the average drag coefficient shows different tendency to Da when $dx = dy = D$ and $dx = dy = 3D$. To better understand the phenomenon, Fig. 7 shows the drag coefficient of each particle at $dx = dy = D$ and $dx = dy = 3D$. i is the serial number of the particles as shown in Fig. 2.

For $dx = dy = D$, it can be seen that the drag coefficient of each particle at $Da = 10^{-2}$ is basically the same as $Da = 10^{-4}$ and for $dx = dy = 3D$, the drag coefficient of all particles at $Da = 10^{-4}$ are evidently larger than those at $Da = 10^{-2}$. As a result, at $dx = dy = 3D$, the average drag coefficient at $Da = 10^{-2}$ is significantly smaller than that at $Da = 10^{-4}$. In addition, C_D of the particles decreases as p increases. Comparing Fig. 7a with b, when $dx\ (dy)$ increases to $3D$, C_D of particles at $p = 1$ decreases and C_D at $p = 2$ increases. It is

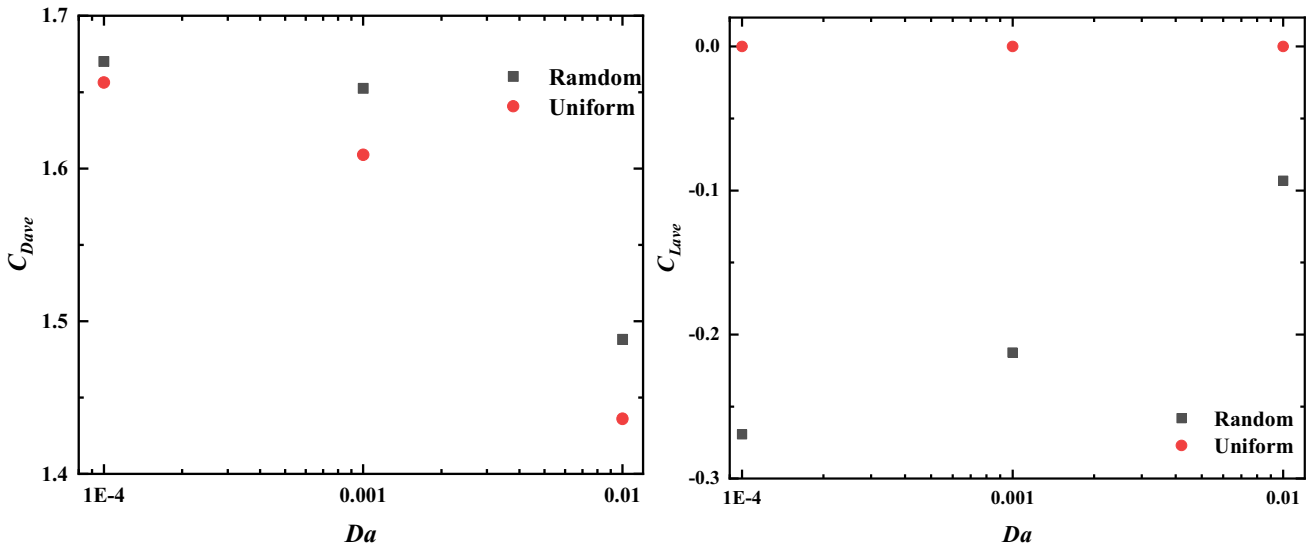

(a) average drag coefficient (b) average lift coefficient

Fig. 12 The **a** average drag coefficient and **b** average lift coefficient of nine identical porous particles for a specific random distribution and uniform distribution at $Re = 20$

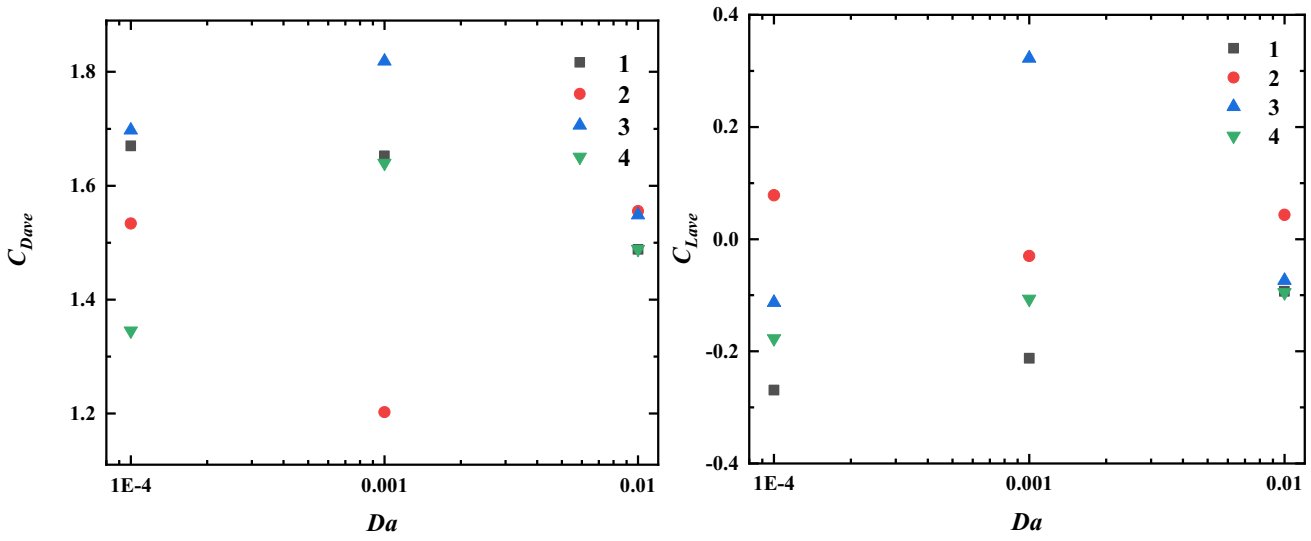

(a) average drag coefficient (b) average lift coefficient

Fig. 13 The **a** average drag coefficient and **b** average lift coefficient of nine identical porous particles for four times random distributions at $Re = 20$

noticed that positive or negative of the drag coefficient means that the direction of the force is different. Therefore, for $p = 3$, the force exerted on the particles changes in direction and the magnitude decrease.

Because the particles are uniformly distributed and symmetric about the y axis, the average lift coefficient of the particles equals zero. But for the lift coefficient of every particle, not all equals zero. Figure 8 indicates the lift coefficient of the nine identical porous particles at $Re = 20$ for $dx = dy = D$ and $dx = dy = 3D$. The particles at $q = 2$ is at the symmetric axis in y direction, the lift coefficients equal zero. At $dx = dy = D$, the lift coefficients of #1 and #7 for $Da = 10^{-2}$ is a little larger than those for $Da = 10^{-4}$. C_L of #2, #3, #8 and #9 at $Da = 10^{-2}$ is the same as that at $Da = 10^{-4}$. In addition, the lift forces exerted on particles at the $q = 1$ and $q = 3$ are opposite. At $q = 1$, the direction of the lift force is downward. Therefore, the cluster has the tendency to gather together more. When dx (dy) increases to $3D$, C_L

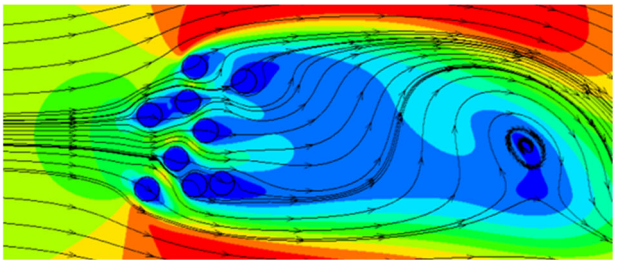

(a) same Da (Da=10^{-3}) and same D (D=40)

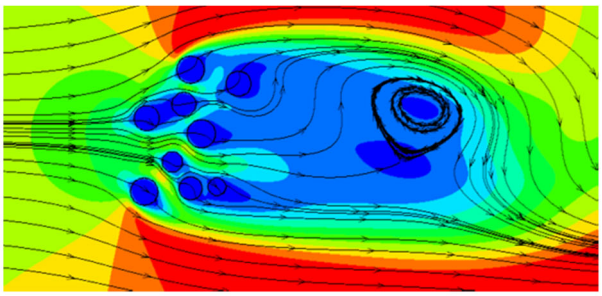

(b) same Da (Da=10^{-3}) and different D

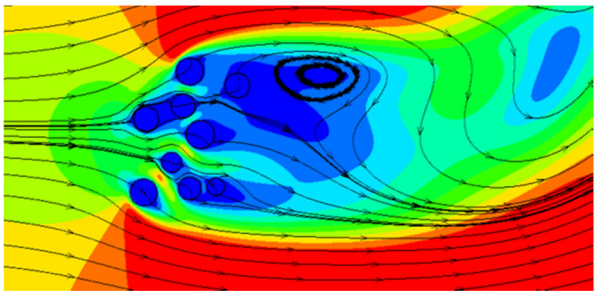

(c) different Da and different D

Fig. 14 Fluid flow around and through nine porous particles for a specific random distribution under different particles conditions

of the particles at $q = 1$ and $q = 3$ for $Da = 10^{-2}$ is smaller than those for $Da = 10^{-2}$. Furthermore, the lift forces exerted on particles at the $q = 1$ and $q = 3$ are also opposite, but the direction of the lift force is upward at $q = 1$, which indicates the particles tend to disperse.

3.1.3 The streamlines analysis with $dx \neq dy$

In order to discuss the influences of the distance between the particles in x and y direction, following we consider the case of $dx \neq dy$. The range of $dx(dy)$ is from 0.25 to 4.0. When $dx = D$, $dx(dy)$ varies from 0.25 to 1.0; when $dy = D$, $dx(dy)$ varies from 1.0 to 4.0. Figure 9 depicts the streamlines of nine identical porous particles at $Re = 20$ and $Da = 10^{-3}$ for $dx(dy) = 0.5$ and $dx(dy) = 2.0$. Compared with Fig. 4a, it is observed under the same Re and Da, when dy increases to $2D$ (Fig. 9a), the wakes behind the cluster vanish but wakes appear behind the particles of $p = 3$. Most fluid flow through the gap between the particles in y direction. When dx increases to $2D$ (Fig. 9b), the flow field resembles to Fig. 4a to some degree. And at the gap between $p = 2$ and $p = 3$, there exist two vortices. Besides, area covered by the wakes extends to the inside of the particles.

3.1.4 The average drag coefficient analysis with $dx \neq dy$

At the same time, the average drag coefficient for different values of Da and $dx(dy)$ is shown in Fig. 10. As $dx(dy)$ increases, the average drag coefficients increase for $0.25 \leq dx(dy) \leq 0.33$; then it drop dramatically and reach a minimum when $dx(dy)$ increases to 1.0; for $1.0 \leq dx(dy) \leq 4.0$, increase slightly. That indicates the distance change in the y direction has more significant impact on the average drag coefficient. For instance, for $Da = 10^{-4}$ and $Re = 20$, at $dx = D$, when dy increases from $2D$ to $3D$, C_{Dave} increases by 5.79%; at $dy = D$, when dx increases from $2D$ to $3D$, C_{Dave} increases by 2.61%. When$dx(dy)$ increases to 1.0, the flow pattern changes dramatically and the average drag coefficient drop greatly. Under the same $dx(dy)$, with Da increasing, C_{Dave} decrease for $0.25 \leq dx(dy) \leq 0.5$; and increase for $1.0 \leq dx(dy) \leq 4.0$.

3.2 Particles with random distribution within a certain region

3.2.1 The particles with the same Darcy number and diameter

In reality, particles are rarely uniformly distributed as discussed above, so following we will discuss the situation that particles are randomly distributed. Firstly, fluid flow around and through nine randomly distributed porous particles with the same diameter and Darcy number was considered. In order to compare with the results of the uniform distribution ($dx = dy = 4D$), the distribution of particles is restricted within a certain range. Figure 11 shows two kinds of streamlines under random spatial distributions. It can be seen that despite under the same Darcy number and Reynolds number, the distribution of porous particles is quite different. Therefore, the characteristics of the flow pattern are also completely different: for Fig. 11a, there is a large vortex at a certain distance behind the porous particles; but for Fig. 11b, there are only two small vortices behind the two porous particles.

First of all, the particles have a specific random distribution (Fig. 11a) and we analyze the relationship between the average drag/lift coefficient and Darcy number. The average drag coefficient and average lift coefficient of nine identical porous particles with random distribution and uniform distribution ($dx = dy = 4D$) at $Re = 20$ for different values of Da are depicted in Fig. 12. It is observed that for a specific

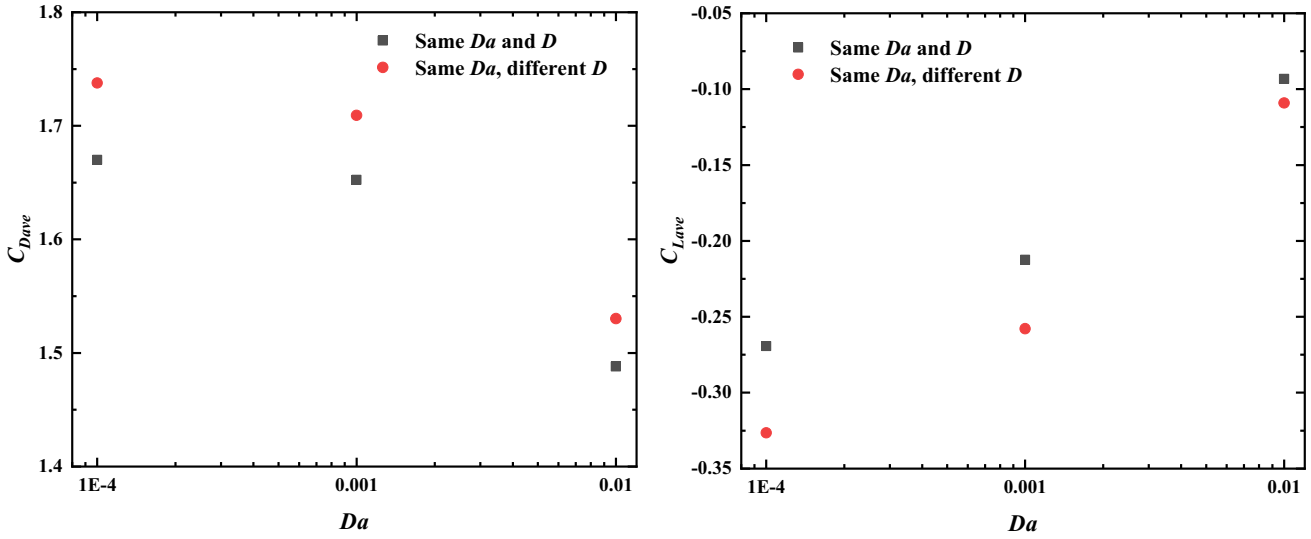

(a) average drag coefficient (b) average lift coefficient

Fig. 15 The **a** average drag coefficient and **b** average lift coefficient of nine particles for a specific random distribution with different D

random distribution, when Da increases, the average drag coefficient decreases which is the same as the uniform distribution. C_{Dave} of the random distribution is larger than that of the uniform distribution and with Da increasing, the difference between them becomes larger. Because the particles' distribution is irregular, the average lift coefficients don't equal zero. As indicated in Fig. 12b, for the specific random distribution, the direction of the total lift force exerted on the nine particles is downward and C_{Lave} decreases with the increase of the Da.

Figure 13 shows the average drag coefficient and average lift coefficient of the particles for random distributions. Four random distribution simulations are performed for each Darcy number ($Da = 10^{-4}$, 10^{-3} and 10^{-2}). It is observed that the average drag and lift coefficient change irregularly when Da increases and although under the same Da, the four random simulations of C_{Dave} and C_{Lave} are very different. Because the randomly distributed particles cause irregular flow field characteristics shown in Fig. 11.

3.2.2 The particles with different Darcy numbers or diameters

In the section, fluid flow around nine randomly distributed particles with random Da or D was investigated. The fluid has the same inlet velocity as discussed above. The particles' diameter varied from 30 to 50 and the Darcy number varies from 10^{-6} to 10^{-2}. Figure 14 shows the streamlines for a specific random distribution. The porous particles have the same D and Da ($D = 40$, $Da = 10^{-3}$) in Fig. 14a, the same Da ($Da = 10^{-3}$) and different diameters in Fig. 14b and different Da and different diameters in Fig. 14c. It is also noted that the diameters of porous particles in Fig. 14c are the same as those in Fig. 14b. Comparing Fig. 14a, b with c, when the diameters or Darcy number of porous particles change, the overall flow pattern is similar-one vortex is formed at a certain distance behind the particles. However, the position of the vortex has changed. Comparing Fig. 14a with b, when the diameters change, the vortex moves to the upper left. Comparing Fig. 14b with c, when the Darcy numbers change, the vortex moves to the upper left further.

The average drag and lift coefficient of nine particles for a specific random distribution with different D is depicted in Fig. 15. In order to compare with the results of particles with the same Da and D, C_{Dave} and C_{Lave} of the particles with the same Da and D are also shown in Fig. 15. It is observed that despite the particles' diameter are different, for a specific random distribution, the C_{Dave} and C_{Lave} were in a reduction when Da varies from 10^{-4} to 10^{-2} which is the same as the simulation results of the particles of the same Da and D. However, under the same Da, the C_{Dave} and C_{Lave} of the particles with the same Da and different D is larger than those of the particles with the same Da and D.

3.3 Particles with random distribution within the whole computation region

In Sect. 3.2, in order to compare with the results of the uniform distribution, the particles which are randomly distributed in a certain region were studied, and in Sect. 3.3, we expand the distribution range to the whole computation region except the wall boundary to avoid the wall effect.

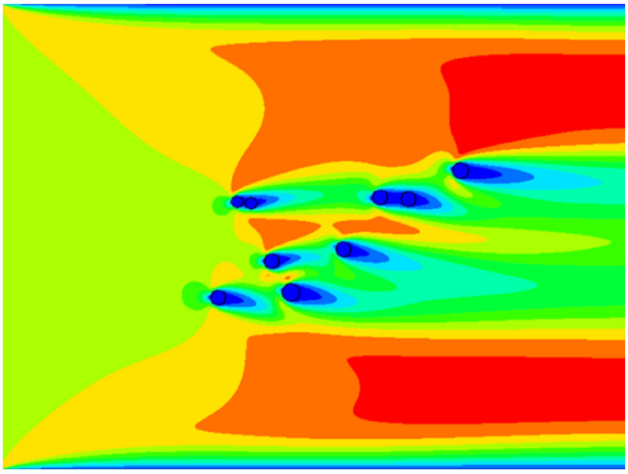

Fig. 16 The flow field of nine particles with different D and Da for a larger random distribution

One simulated flow field is shown as Fig. 16. The particles' diameter and Darcy number are different. It is observed that when the fluid flow through the porous particles, the velocity of the fluid decreases. When particles are close, the behind particle are severely influenced by the low velocity resulting from the front particle. And when the distance between the particles becomes larger, the velocity of the fluid passing through the front particles gradually recovers as it flows to the behind particles.

Figure 17 shows the average drag and lift coefficient for several times random distributions. It can be seen for the seven times random distribution, although every time the particles' diameter and Darcy number are different, there is not much difference between the average drag coefficient. But the average lift coefficient changes greatly. This is because when the region where the particles are randomly distributed is large enough, the porous particles can be completely dispersed in the computational domain. The random spatial distribution of the particles and the random diameter and Darcy number generated by the computer system may have a little effect on the drag coefficient. However, since the distribution of particles is not symmetrical about the y-axis, it will inevitably lead to a large difference in the lift coefficient.

4 Conclusions

Two-dimensional steady flow around and through nine porous particles was investigated numerically. Uniform and random spatial distribution were both considered and the influences of Reynolds number, Darcy number and the distance between particles on the flow characteristics were analyzed in detail. Some important conclusions are summarized as follows:

(1) When $dx = dy = D$, the particles form a cluster which exerts an overall influence on the fluid, and therefore, two recirculating symmetrical wakes are formed behind the cluster. When dx (dy) increases, most fluid flows through the space between the particles with low resistance and this phenomenon is more obvious at low Da.
(2) The average drag coefficient increases as $dx(dy)$ increases, but the growth rate gradually slows down which indicates the influences of $dx(dy)$ decrease.

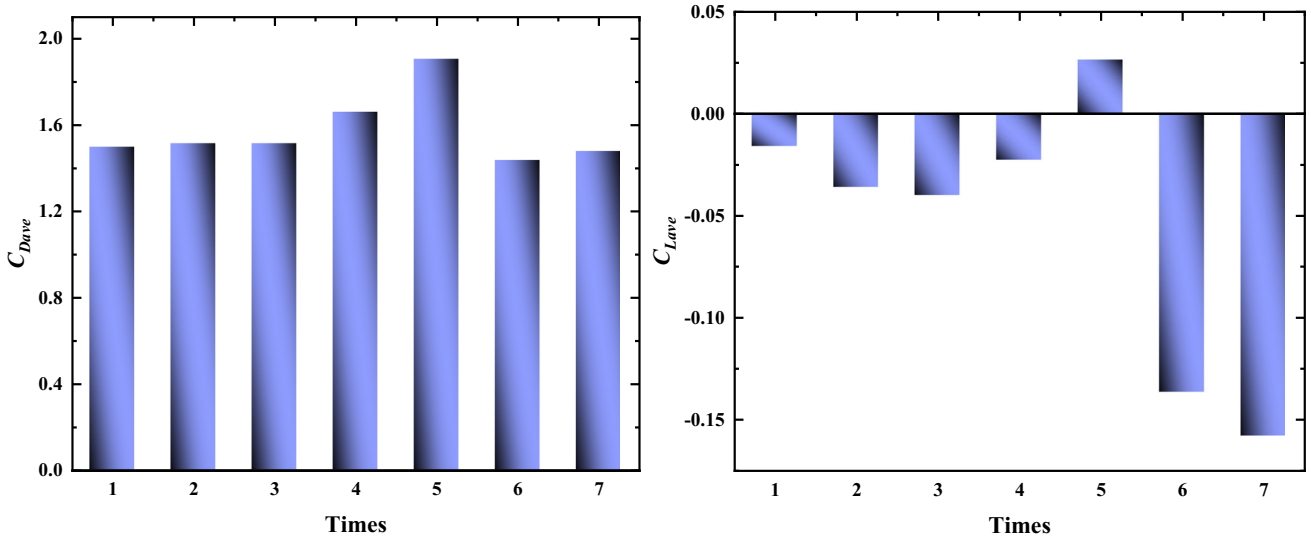

(a) average drag coefficient (b) average lift coefficient

Fig. 17 The **a** average drag coefficient and **b** average lift coefficient of the particle with different D and Da for a larger random distribution

(3) The distance change in y direction has more significant impact on the average drag coefficient. For instance, for $Da = 10^{-4}$ and $Re = 20$, at $dx = D$, when dy increases from $2D$ to $3D$, C_{Dave} increases by 5.79%; at $dy = D$, when dx increases from $2D$ to $3D$, C_{Dave} increases by 2.61%.

(4) The flow field and drag coefficient are closely related to the distribution of particles. For a specific random distribution, the change of average drag coefficient with Da is similar to the uniform spatial distribution. When the region where the particles are randomly distributed is large enough, the random distribution may have little effect on the drag coefficient.

Acknowledgements This work is supported by the National Natural Science Foundation of China (51922086).

Declarations

Conflict of interest The authors declare that there is no conflict of interests.

References

1. Chen RC, Wu JL (2000) The flow characteristics between two interactive spheres. Chem Eng Sci 55(6):1143–1158
2. Tritton DJ (1959) Experiments on the flow past a circular cylinder at low Reynolds numbers. J Fluid Mech 6(4):547–567
3. Bhattacharyya S, Dhinakaran S, Khalili A (2006) Fluid motion around and through a porous cylinder. Chem Eng Sci 61(13):4451–4461
4. Dalman MT, Merkin JH, McGreavy C (1986) Fluid flow and heat transfer past two spheres in a cylindrical tube. Comput Fluids 14(3):267–281
5. Folkersma R, Stein HN, van de Vosse FN (2000) Hydrodynamic interactions between two identical spheres held fixed side by side against a uniform stream directed perpendicular to the line connecting the spheres' centres. Int J Multiph Flow 26(5):877–887
6. He X, Doolen G (1997) Lattice Boltzmann method on curvilinear coordinates system: flow around a circular cylinder. J Comput Phys 134(2):306–315
7. Hsu JP, Yeh SJ (2009) Translation of two rigid spheres perpendicular to their line-of-centers and normal to a plate. Powder Technol 194(1–2):10–17
8. Jin H et al (2019) Numerical investigation on drag coefficient and flow characteristics of two biomass spherical particles in supercritical water. Renew Energy 138:11–17
9. Niu XD et al (2006) A momentum exchange-based immersed boundary-lattice Boltzmann method for simulating incompressible viscous flows. Phys Lett A 354(3):173–182
10. Yu P et al (2011) Steady flow around and through a permeable circular cylinder. Comput Fluids 42(1):1–12
11. O'Brien TJ, Syamlal M (1993) Particle cluster effects in the numerical simulation of a circulating fluidized bed. In: Avidan A (ed) Circulating fluidized bed technology IV, Hidden Valley, 1993. AIChE, New York, pp 345–350
12. Sandeep KP, Zuritz CA (1996) Drag on multiple sphere assemblies suspended in non-newtonian tube flow. Blackwell Publishing Ltd, Oxford, pp 171–183
13. Beetstra R, van der Hoef MA, Kuipers JAM (2006) A lattice-Boltzmann simulation study of the drag coefficient of clusters of spheres. Comput Fluids 35(8–9):966–970
14. Shah MT et al (2013) Effect of a cluster on gas–solid drag from lattice Boltzmann simulations. Chem Eng Sci 102:365–372
15. Wei X, Weber J, Breault RW (2021) Numerical investigation of the penetrating gas flow into particle clusters for circulating fluidized beds. Powder Technol 388:442–449
16. Rong FM et al (2011) Numerical simulation of the flow around a porous covering square cylinder in a channel via lattice Boltzmann method. Int J Numer Meth Fluids 65(10):1217–1230
17. Tang Y, Liu H (2017) Modeling multidimensional and multispecies biofilms in porous media. Biotechnol Bioeng 114(8):1679–1687
18. Nithiarasu P, Seetharamu KN, Sundararajan T (1997) Natural convective heat transfer in a fluid saturated variable porosity medium. Int J Heat Mass Transf 40(16):3955–3967
19. Wang L et al (2015) Volume-averaged macroscopic equation for fluid flow in moving porous media. Int J Heat Mass Transf 82:357–368
20. Qian YH, d'humières D, Lallemand P (1992) Lattice BGK models for Navier-Stokes equation. Europhys Lett 6(17):479–484
21. Nield DA, Bejan A (2006) Convection in porous media
22. Ladd AJC (1994) Numerical simulations of particulate suspensions via a discretized Boltzmann equation. Part 1. Theoretical foundation. J Fluid Mech 271:285–309